A nonlinear meccano for Alzheimer's emergence by amyloid β-mediated glutamatergic hyperactivity

Giulio Bonifazi [a,b,c], Celia Luchena [b,d,e], Adhara Gaminde-Blasco [b,d,e], Carolina Ortiz-Sanz [b,d,e], Estibaliz Capetillo-Zarate [b,d,e], Carlos Matute [b,d,e], Elena Alberdi [b,d,e], Maurizio De Pittà [a,b,c,f,*]

[a] Basque Center for Applied Mathematics, Alameda Mazarredo 14, Bilbao 48009, Bizkaia, Spain
[b] Department of Neurosciences, University of the Basque Country, Barrio Sarriena, s/n, Leioa 48940, Bizkaia, Spain
[c] Krembil Research Institute, University Health Network, 60 Leonard Ave, Toronto M5T 0S8, ON, Canada
[d] Achucarro Basque Center for Neuroscience, Barrio Sarriena, s/n, Leioa 48940, Bizkaia, Spain
[e] Centro de Investigación Biomédica en Red en Enfermedades Neurodegenerativas (CIBERNED), Barrio Sarriena, s/n, Leioa 48940, Bizkaia, Spain
[f] Department of Physiology, University of Toronto, 1 King's College Circle, Toronto M5S 1A8, ON, Canada

ARTICLE INFO

ABSTRACT

The pathophysiological process of Alzheimer's disease (AD) is believed to begin many years before the formal diagnosis of AD dementia. This protracted preclinical phase offers a crucial window for potential therapeutic interventions, yet its comprehensive characterization remains elusive. Accumulating evidence suggests that amyloid-β (Aβ) may mediate neuronal hyperactivity in circuit dysfunction in the early stages of AD. At the same time, neural activity can also facilitate Aβ accumulation through intricate feed-forward interactions, complicating elucidating the conditions governing Aβ-dependent hyperactivity and its diagnostic utility. In this study, we use biophysical modeling to shed light on such conditions. Our analysis reveals that the inherently nonlinear nature of the underlying molecular interactions can give rise to the emergence of various modes of hyperactivity. This diversity in the mechanisms of hyperactivity may ultimately account for a spectrum of AD manifestations.

1. Introduction

The clinical course of Alzheimer's disease (AD) starts with the appearance of the first symptoms of mild cognitive impairment (MCI) (Morris et al., 2001). These symptoms then slowly progress to dementia as deficits emerge in multiple cognitive domains that are severe enough to produce loss of function (Jack Jr et al., 2010). Well-known neuropathological correlates of the disease are extracellular amyloid-β (Aβ) accumulations and intracellular depositions of neurofibrillary tangles in association with neurodegeneration by neuronal and synaptic loss reflected by progressive brain atrophy (Blennow and Zetterberg, 2018; Olsson et al., 2016; Huijbers et al., 2015; Jack Jr et al., 2011).

The progression from MCI to dementia cannot be reverted at present, making AD intractable and the most common cause of dementia in elderly people (Kelley et al., 2015). On the other hand, Aβ and neurofibrillary tangles buildup could start long before MCI onset (Jack Jr. et al., 2010, 2009), pinpointing the existence of a preclinical phase of AD that most likely sets its fate, namely if, and to what extent, AD clinical features will develop (Sperling et al., 2011). Thus, to predict the risk of

developing dementia by Alzheimer's, characterizing the preclinical phase of the disease is crucial.

Current biomarker models of AD's preclinical phases do not effectively predict the clinical syndrome of AD (Sperling et al., 2011). Aβ accumulation, for example, is recognized as a key early biomarker in AD etiology that is necessary yet likely insufficient to incite the disorder's downstream pathological cascade (Frisoni et al., 2022; Jack Jr et al., 2010). Hence, efforts are in the direction of identifying additional biomarkers that could predate Aβ accumulation or that, in combination with it, could predict the risk of developing the disease's clinical syndrome reliably (Frisoni et al., 2022; Frisoni et al., 2020).

Several lines of evidence indicate that neuronal hyperactivity could also be a harbinger of AD-related dementia (Zott and Konnerth, 2023; Harris et al., 2020). Functional imaging studies in individuals with prodromal AD such as MCI reveal increased neuronal activity in the hippocampus and some neocortical areas (Huijbers et al., 2015; Mormino et al., 2012; Quiroz et al., 2010; Dickerson et al., 2005; Bookheimer et al., 2000), and those individuals often suffer from epileptic seizures possibly resulting from such excessive neuronal activation

---

(Vossel et al., 2013; Palop and Mucke, 2009). Significantly, reducing hippocampal hyperactivation in MCI patients using the antiepileptic drug levetiracetam can partially restore cognitive function, especially in those patients also suffering from epileptic seizures (Vossel et al., 2021; Bakker et al., 2015; Bakker et al., 2012).

A growing body of clinical observations supported by experiments in AD-related mouse models pinpoint the disequilibrium between neuronal excitation and inhibition (E/I balance) as the biophysical mechanism for prodromal neural hyperactivity in AD (Harris et al., 2020; Palop and Mucke, 2010). Among the potential genetic, molecular, and cellular factors that could cause such E/I imbalance, Aβ deposition is known to disrupt the blood-brain barrier and induce metabolic dysfunction (Nation et al., 2019; Sweeney et al., 2018; Bass et al., 2015), reduce inhibitory GABAergic neurotransmission, and modulate the expression of multiple channels that regulate intrinsic neuronal excitability (Targa Dias Anastacio et al., 2022; Harris et al., 2020; Palop and Mucke, 2016). More recently, however, the extracellular accumulation of soluble Aβ oligomers predating Aβ deposition has also been shown to induce hyperactivity (Keskin et al., 2017; Busche et al., 2012). The presence of soluble Aβ in the extracellular space in the early stages of AD can reduce the expression of astrocytic GLT1 transporters (Zott et al., 2019; Hefendehl et al., 2016; Scimemi et al., 2013). Since these transporters are the main ones responsible for the clearance of extracellular glutamate (Danbolt et al., 2016), a reduction in their expression would result in a decreased uptake accounting for extracellular glutamate buildup that induces neuronal hyperactivation (Rothstein et al., 1996).

Because Aβ production is activity-dependent (Cirrito et al., 2005; Kamenetz et al., 2003), so is Aβ-dependent GLT1 reduction, and the resulting glutamate buildup (Zott et al., 2019). More extracellular glutamate then increases neuronal firing, which, in turn, promotes further glutamate release from synaptic terminals and Aβ production. In this fashion, a positive feedback loop is in place whereby initially low extracellular levels of Aβ and glutamate could be increased by ongoing neural activity and, in turn, increase the latter exacerbating AD clinical progression (Zott and Konnerth, 2023; Zott et al., 2019).

The activity requirements of this feedback loop, however, are not understood. Preexisting baseline neural activity is necessary to promote Aβ-dependent hyperactivity (Zott et al., 2019), but what levels of such
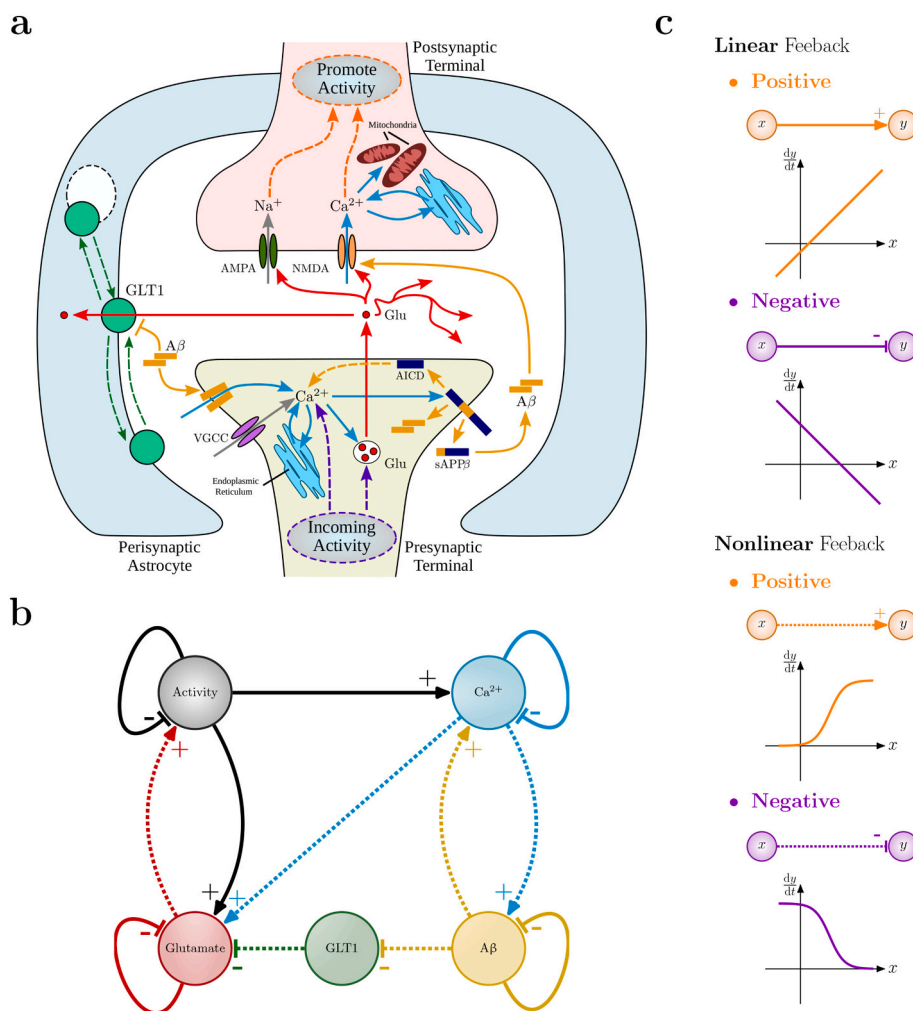

Fig. 1. Aβ -dependent regulation of extracellular glutamate. **a** Molecular pathways regulating extracellular glutamate in the presence of Aβ accumulation. In healthy tissue, astrocytic glutamate transporters (GLT1) take up the majority of synaptically-released glutamate, shaping postsynaptic currents and regulating local neural activity. GLT1 expression, however, can change with extracellular Aβ in a diverse fashion that depends on neural intracellular Ca^{2+} (Zott and Konnerth, 2023; Scimemi et al., 2013). Intracellular Ca^{2+} can elicit the secretory cleavage of the amyloid precursor protein (sAPP) both by activity-dependent and independent mechanisms (Bezprozvanny and Mattson, 2008). sAPPβ monomers are further cleaved by β-secretase into soluble Aβ peptides that aggregate into insoluble fibrils and deposit as amyloidogenic plaques (Viola and Klein, 2015). At the same time, Aβ and intracellular APP domains (AICD) can promote Ca^{2+} signaling through various intracellular and extracellular pathways (Gallego Villarejo et al., 2022). **b** Model of extracellular glutamate homeostasis including Aβ-dependent GLT1 regulation. Such regulation is by the interaction of activity-dependent glutamate release with Ca^{2+}-dependent Aβ production, which is mediated by multiple loops of nonlinear interactions illustrated in **c**.

baseline activity could hasten the latter are unclear (Zott and Konnerth, 2023). At the same time, the fact that not all AD patients with Aβ pathology develop seizures (Larner and Doran, 2006), nor all individuals with Aβ-correlated seizures develop AD (Mackenzie and Miller, 1994), suggests that the combination of Aβ buildup with neuronal hyperactivation predating the clinical phase of AD is variegated. Here, we explore this hypothesis, building a mathematical model of Aβ-dependent hyperactivity that considers the time-dependent expression of possible biomarkers associated with the phenomenon, such as extracellular Aβ and glutamate concentrations, and neuronal firing (Carter et al., 2019; Blennow and Zetterberg, 2018; Vossel et al., 2017; Busche and Konnerth, 2016).

To model biomarkers' temporal evolution, we consider three critical molecular pathways underpinning Aβ-dependent hyperactivity (Zott and Konnerth, 2023): (i) glutamate-mediated neuronal activity, (ii) Aβ-dependent glutamate uptake, and (iii) activity-dependent Aβ production (Fig. 1a). The molecular reactions mediating such pathways and their interactions are nonlinear. Hence, a change in biomarker expression ensuing from a perturbation of one pathway is generally not proportional to that perturbation, nor can the singly perturbed pathway be accounted for. Instead, it is the result of combining the latter with the other interacting pathways. Moreover, the interactions among the different molecular pathways can mediate multiple positive feedback loops (Fig. 1b). In such a scenario, the theory of nonlinear dynamical systems predicts that multiple biomarker expressions could co-exist for the same preclinical stage of AD (Pisarchik and Feudel, 2014). We interpret this possibility by the existence of multiple trajectories towards clinical AD manifestations, each possibly associated with a specific risk of developing MCI and dementia.

2. Results

2.1. Uptake by astrocytic transporters is the limiting process in extracellular glutamate clearance around Aβ accumulations

Aβ-dependent hyperactivity in preclinical AD is rarely whole-brain (Zott and Konnerth, 2023; Vossel et al., 2013). Instead, it is distributed and co-localizes microscopically with extracellular Aβ-depositions, also known as plaques, which are an early and predictive marker for the possible progression of preclinical to symptomatic AD (Jagust, 2018;

Morris et al., 2009). Before plaque deposition, however, soluble Aβ must accumulate at the plaque site, hastening plaque deposition (Hefendehl et al., 2011; Hong et al., 2011). At the same time, as the plaque forms and grows, soluble Aβ continuously binds and unbinds from its surface, generating a toxic microenvironment around the plaque site where neuronal hyperactivity emerges (Busche et al., 2012; Busche et al., 2008).

Imaging of synaptically evoked extracellular glutamate transients nearby Aβ plaques hints at reduced glutamate clearance rates by astrocytic transporters as a putative biophysical correlate for the toxic nature of the plaque microenvironment (Hefendehl et al., 2016). It is helpful to understand how this happens in terms of the physical laws governing extracellular glutamate signaling. To this extent, we consider a tissue ball in the proximity of a plaque where we expect soluble Aβ accumulations as a model of the tissue microenvironment around the plaque (Figs. 2a,b and Appendix A). How large our ball is in radius R will depend on the Aβ gradient under consideration, reflecting the extent of the plaque's toxic microenvironment (Hefendehl et al., 2016). Typical radii are in the range of tens of micrometers (Querol-Vilaseca et al., 2019; Hefendehl et al., 2016; Pickett et al., 2016; Hefendehl et al., 2011), thus much larger than individual synapses whose maximum dimension usually is of the order of tens of nanometers (Figs. 2c,d) (Curran et al., 2021; Shapson-Coe et al., 2021; Kasthuri et al., 2015).

Our tissue ball will generally comprise multiple cell bodies, dendrites, synapses, and astrocytic processes that are part of active neural circuits. We can characterize the geometry of the extracellular space associated with those circuits by the average fraction (α) of extracellular volume with respect to the ball volume. We also consider the average shape of the extracellular space in the ball as reflected by the tortuosity (λ) of the path of extracellular molecules diffusing around cellular obstructions created by the neuropil structure in the ball. The advantage of introducing these quantities is to be able to describe extracellular glutamate in time (t) and space ($\mathbf{x}$) in the plaque microenvironment, i.e., $g(\mathbf{x}, t)$, by the macroscopic balance of synaptic release, $J_{\text{syn-rel}}(\alpha)$, with clearance by passive diffusion, $J_{\text{diff}}(g, \lambda)$, and active uptake by astrocytic transporters, $J_{\text{uptake}}(g, \alpha)$ (Bergles et al., 1999). Namely (Syková and Nicholson, 2008)

$$\frac{\partial}{\partial t} g(\mathbf{x}, t) = J_{\text{syn-rel}}(\alpha) + J_{\text{diff}}(g, \lambda) - J_{\text{uptake}}(g, \alpha) \tag{1}$$
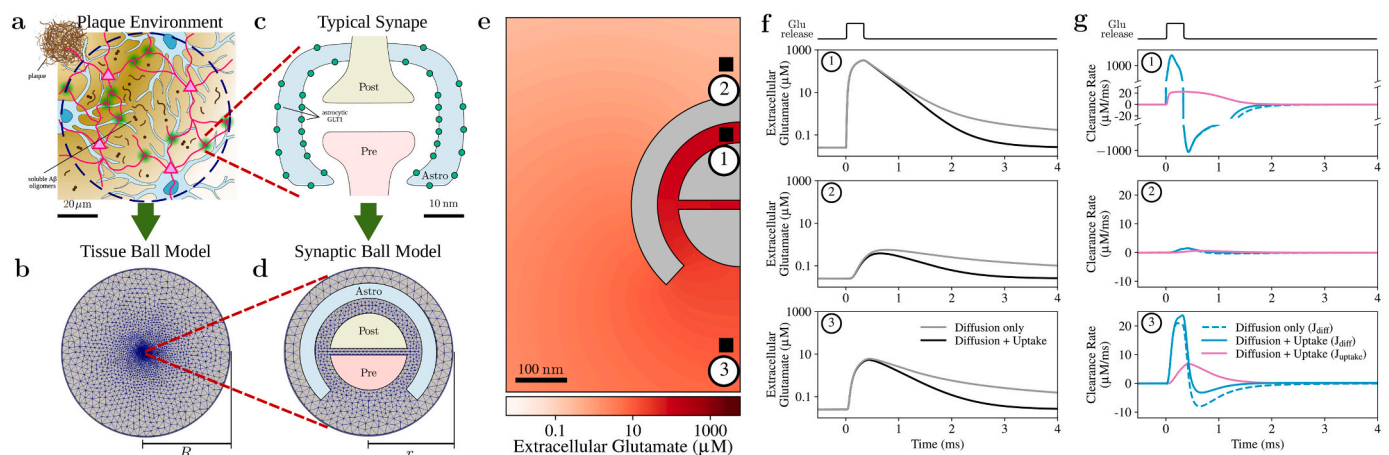

Fig. 2. Contribution of astrocytic transporter uptake to extracellular glutamate clearance. **a,b** Model of the plaque microenvironment. The microenvironment in the proximity of an Aβ plaque is described by a tissue ball of radius R containing multiple synapses and astrocytes surrounded by an extracellular milieu that is rich in soluble Aβ. **c,d** Typical synapses in this ball have much smaller radial size r and consist of pre- and postsynaptic terminals ensheathed by GLT1-expressing astrocytic processes. **e** Snapshot of the spatial distribution of perisynaptic glutamate taken 300 μs after a pulsed glutamate injection at the synapse center. **f** Associated glutamate time course at three sample points in the perisynaptic space (*black traces*). Compared with the time course in the absence of GLT1 uptake (*gray*), it may be appreciated how the uptake by astrocyte transporters reduces the transient duration of extracellular glutamate excess. **g** Considering the time evolution of the glutamate clearance by diffusion only vs. diffusion plus uptake reveals how diffusion is only marginally affected by uptake. That is, uptake by astrocytic transporters, rather than diffusion, modulates how fast extracellular glutamate is cleared.

It is enlightening to look at solutions of the above equation in the surroundings of what a typical synapse could look like in our tissue ball (Lehre and Rusakov, 2002; Rusakov and Kullmann, 1998) (Fig. 2e and Appendix A). Consider, for example, a brief glutamate injection at the center of the synaptic cleft mimicking synaptic release for $0 < t \leq 0.3$ (near point "1" in Fig. 2e). Eq. (1) predicts a redistribution of this initial glutamate surge from the cleft to the extrasynaptic space by diffusion. The rise of extracellular concentration at any point in space is location-dependent due to synaptic and astrocytic obstacles (Fig. 2f). On the other hand, for $t > 0.3$, clearance of extracellular glutamate is qualitatively similar everywhere, either in the presence of or without uptake by astrocytic transporters (Fig. 2f, dark vs. light gray traces). The existence of uptake by transporters shortens the time course of extracellular glutamate. However, looking at individual mechanisms setting such time course (Fig. 2g), it may be appreciated how glutamate uptake mainly contributes to the initial phase of glutamate clearance, and only when the local glutamate concentration is high enough. This follows from the sigmoid nonlinearity $\mathscr{H}_1(g, K_U) = \frac{g}{g + K_U}$ rising from the Michaelis-Menten-type kinetics of glutamate uptake (Tzingounis and Wadiche, 2007; Rusakov and Kullmann, 1998), whereby

$$J_{\text{uptake}}(g, \alpha) = \widehat{J}_U(\alpha) \mathscr{H}_1(g, K_U) \tag{2}$$

Eq. (2) tells us that J_{uptake} is nonnegligible only when glutamate concentration approaches or exceeds the transporter's affinity K_U, that is, approximately, when $0.1 K_U < g < 0.5 K_U$. When extracellular glutamate concentration largely exceeds K_U instead, e.g., $g > 10 K_U$, J_{uptake} saturates to the maximum uptake rate $\widehat{J}_U(\alpha)$. In this fashion, the maximal rate of glutamate clearance ensuing from diffusion and uptake cannot exceed $J_{\text{diff}}(g, \lambda) + \widehat{J}_U(\alpha)$. Therefore, since uptake but not diffusion changes with Aβ (Hefendehl et al., 2016), we conclude that uptake by astrocytic transporters is the mechanism that sets the limit for the shortest possible time course of extracellular glutamate in the synaptic cleft and extrasynaptically in the plaque microenvironment.

2.2. The nonlinear nature of glutamate uptake results in nonuniform activity-dependent regulation of extracellular glutamate in the Aβ plaque microenvironment

The existence of a maximum clearance rate also implies that a maximum rate of glutamate supply to the extracellular space must exist beyond which glutamate starts accumulating extracellularly. This could happen, for example, when many synapses in our tissue ball are active for a protracted period and can be accounted for by a glutamate supply, $J_{\text{syn-rel}}$ in Eq. (1), that is proportional to the neural activity rate (Appendix B). Then, glutamate supply will exceed clearance for sufficiently large activity rates, promoting extracellular glutamate accumulation.

The activity rate promoting extracellular glutamate buildup will depend on the maximum uptake rate ($\widehat{J}_U$). Astrocytic excitatory amino acid transporters – EAAT2 in humans and GLT1 in murine tissue – account for the majority of glutamate uptake in the adult brain, allowing neglecting the contribution to uptake by other transporter types (Tzingounis and Wadiche, 2007; Danbolt, 2001; Bergles and Jahr, 1998). We can thus assume that all transporters equally contribute to glutamate uptake in our tissue ball and estimate the maximum uptake rate by the product of the single transporter uptake rate (r_{GLT1}) by the average transporter concentration ($n(\alpha)$) found in our tissue ball. This concentration, and so the associated uptake rate, is the highest in the healthy tissue ($\widehat{n}(\alpha)$) while progressively reducing with Aβ accumulation (Hefendehl et al., 2016; Scimemi et al., 2013). We can conveniently express this fact by

$$\widehat{J}_U(\alpha) = \gamma \widehat{n}(\alpha) r_{\text{GLT1}} \tag{3}$$

where the healthy tissue scenario corresponds to $\gamma = 1$ when the maximum uptake rate is the fastest because transporter expression is the largest, namely, $\widehat{J}_U = \widehat{n} \cdot r_{\text{GLT1}}$. Conversely, when $0 \leq \gamma < 1$, a decrease in transporter expression and thus in uptake is envisaged by the presence of extracellular Aβ and we look at this scenario for the emergence of toxic extracellular glutamate accumulations.

In Figs. 3a,b, we consider extrasynaptic glutamate dynamics for different transporter expression at two sample rates (ν) of synaptic release in the gamma frequency range that could be representative of cognitive-relevant neural activity in our tissue ball (Fries et al., 2007; Buzsaki, 2006). On the upper end of the spectrum of transporter expression, when $\gamma = 1$, our simulations predict that extrasynaptic glutamate will generally transiently accumulate in the range of $1 - 150$ μM (pink traces in Fig. 3b). Though considerably higher than resting extracellular glutamate levels reported to be < 0.1 μM (Herman and Jahr, 2007; Cavelier and Attwell, 2005), these concentrations agree with estimates of non-toxic physiological glutamate levels surrounding active synapses (Lehre and Rusakov, 2002; Barbour, 2001; Clements et al., 1992). Conversely, on the lower end of the uptake spectrum, in conditions of strongly reduced transporter expression ($\gamma = 0.1$), we find instead dangerously high glutamate concentrations, i.e., > 200 μM (dark red traces in Fig. 3b). Glutamate concentrations of such magnitude are estimated to mediate acute and chronic excitotoxicity (Lewerenz and Maher, 2015).

We observe healthy and toxic microenvironments for the same transporter expression ($\gamma = 1$ and $\gamma = 0.1$, respectively) regardless of the activity rate under consideration. However, this would not be the case for an intermediate ($\gamma = 0.5$) reduction of transporter expression. In such a scenario, it may be appreciated how glutamate reaches physiological concentrations ≤ 150 μM for $\nu = 20$ Hz but builds up to toxic levels > 1500 μM that are 10-fold larger, for just a 2.5-fold increase in activity when $\nu = 50$ Hz. This asymmetric increase of extracellular glutamate with respect to the activity rate follows from the nonlinearity of Eq. (1) introduced by the transporter kinetics, whereby the glutamate uptake rate saturates for $20 < \nu < 50$ Hz. Thus, at $\nu = 50$ Hz, but not at 20 Hz, glutamate supply ($J_{\text{syn-rel}}$) exceeds clearance, allowing for the quick buildup of toxic concentrations.

The asymmetric nature of activity-dependent glutamate accumulation tells us that the activity requirements to develop toxic glutamate accumulations in the plaque microenvironment change with different transporter expressions and that the way they change and the associated risk of glutamate toxicity are nonuniform. We can appreciate such a nonuniformity by mapping how the average extracellular glutamate concentration (Fig. 3c) changes with increasing activity and the rate at which that change occurs (Fig. 3d) for multiple transporter expressions in our tissue ball. It may be seen how toxic glutamate concentrations can only be attained beyond a threshold activity rate that varies with transporter expression (Fig. 3c, right inset). Such a threshold can be inferred from the sigmoid curve fitting the estimated slope of the average glutamate concentration curve (Fig. 3d, right inset). Additionally, the fact that such slope is sigmoid hints that extracellular glutamate nonlinearly increases with increasing baseline synaptic activity, as would be the case for emerging Aβ-dependent hyperactivity (Zott et al., 2019). The glutamate increase indeed approaches zero for small increments of synaptic release at low baseline activity but progressively grows towards a maximum when such baseline increases. We can also regard the rate of change in glutamate buildup for increasing synaptic activity as an estimation of the sensitivity, and thus the risk (Frey and Sumeet, 2002), for those buildups to grow toxic. In this framework, the risk of developing glutamate toxicity will nonuniformly change along the sigmoid derivative by the dynamic modulation of the release threshold as transporter expression reduces with accumulating Aβ (Tong et al., 2017; Scimemi et al., 2013).
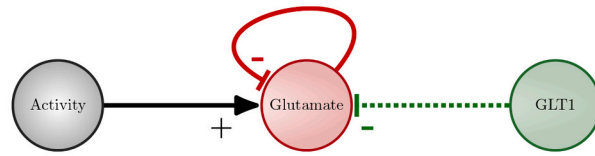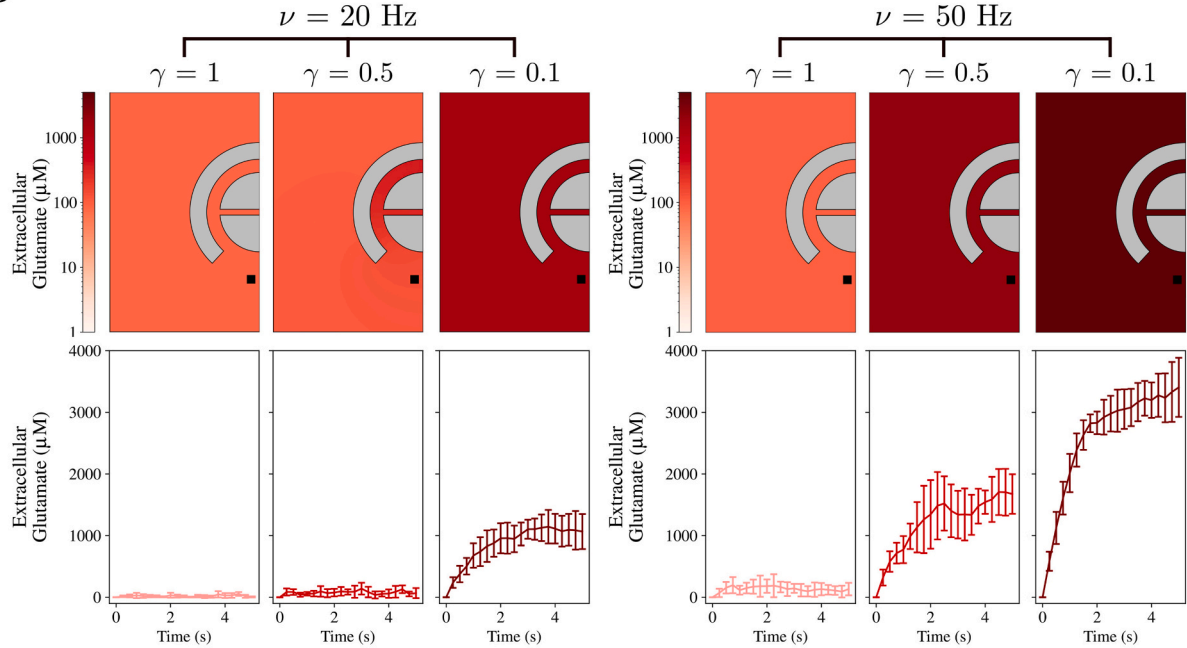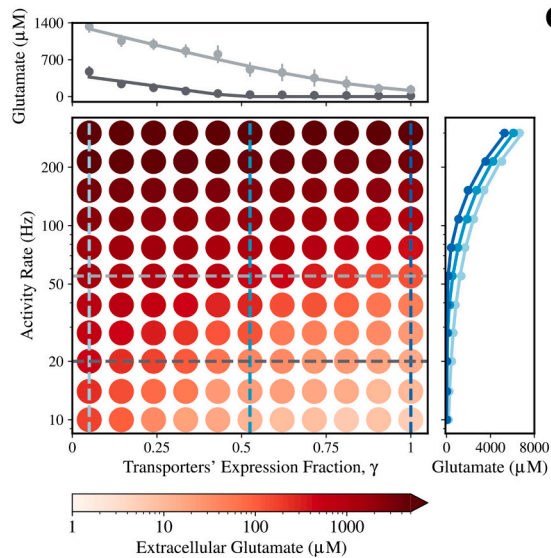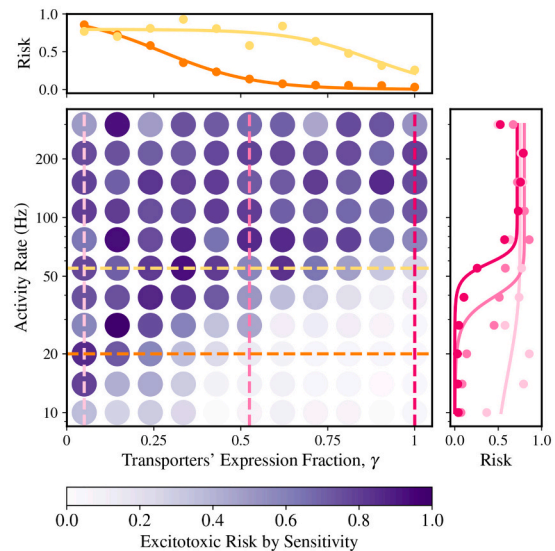
Fig. 3. Nonlinear extracellular glutamate accumulation. **a** Model setup to characterize how activity-dependent synaptic release influences extracellular glutamate clearance. **b** Simulated perisynaptic glutamate levels for Poisson-distributed glutamate pulse injections at the synapse center at two rates (ν) representative of sensory-relevant synaptic activity and for different expressions of astrocytic glutamate transporters (γ). The *top* panels are snapshots of extracellular glutamate at $t = 5$ s around a typical microenvironment synapse, averaged over $n = 20$ simulations. The *bottom* panels show the average glutamate time course ($\pm$s.t.d.) at the location marked by the *black square* in the top panels. **c** Average steady-state extracellular glutamate in the plaque microenvironment as a function of γ and ν. (*Insets*) Representative curves for steady-state glutamate concentrations attained by fixing γ or ν show a nonlinear behavior marked by an inflection point beyond which glutamate can increase towards potentially toxic levels. **d** Computation of the slope of glutamate concentration with respect to ν at fixed γ provides a measure of how susceptible glutamate is to increase in response to rate variations and thus reflects the risk of developing such toxic glutamate accumulations. (*Insets*) Tracing this risk as a function of ν or γ reveals a sigmoid curve, whose inflection point nonuniformly changes with γ (respectively, ν).

2.3. The threshold for glutamate-mediated neural hyperactivation is complex

In parallel with transporter expression's Aβ-dependent dynamics, an additional dynamical component in the modulation of the activity threshold for the onset of glutamate toxicity comes from the possible time-dependence of synaptic glutamate release by spontaneous or evoked fluctuations in the neural activity in the plaque microenvironment. We can think of this activity as the result of afferent excitation from the outside of the microenvironment (ν_{ex}) in combination with local firing activity (ν) resulting from the balance of two opposite feedback mechanisms (Fig. 4a). One is the positive feedback of extracellular glutamate on neural activity and the synaptic glutamate release associated with it (Zott et al., 2019), which we denote by some generic function $F_{syn-rel}(g)$ for the moment. The other is the negative feedback, likely mediated by multiple molecular pathways that homeostatically maintain a baseline activity (ν_0) in our tissue ball (Frere and Slutsky, 2018). The interplay of these mechanisms can be described by the differential equation

$$\frac{d}{dt}\nu = -\Omega_0(\nu - \nu_0) + F_{syn-rel}(g) \tag{4}$$

The first right-hand side term in the above equation reflects the homeostatic feedback, which we can consider, without loss of generality, to be linear with the difference of the instantaneous local activity rate from baseline, i.e., $\nu - \nu_0$, by the homeostatic recovery rate constant Ω_0 (O'Leary and Wyllie, 2011). However, that is not true for the positive feedback term $F_{syn-rel}$. The fact that neurons can only fire when depolarized beyond a firing threshold by excitatory (glutamatergic) synapses (Rauch et al., 2003) implies that the feedback of extracellular glutamate on neuronal depolarization, and thus firing, and downstream synaptic

release, kicks in only around and beyond a threshold glutamate concentration. The existence of such a threshold may conveniently be described by a sigmoid glutamate-dependent change of the activity rate such as (Appendices C and G)

$$F_{syn-rel}(g) = O_S \cdot \mathcal{H}_1(g, K_S) \tag{5}$$

where K_S is the threshold glutamate concentration for feedback emergence, and O_S is the maximum change rate as extracellular glutamate grows large beyond the threshold, e.g., $g > 10K_S$.

We emphasize the sigmoid nonlinearity introduced by the glutamate-dependent feedback because, together with the nonlinearity of transporters' uptake (Eq. (2)), it could put forth a molecular switch for the onset of glutamate toxicity. We may appreciate this switch in Figs. 4b,c which show representative numerical solutions of Eq. (1) for the time course of the average extracellular glutamate following a transient increase of afferent activity (ν_{ex}, top pulses, for $0 \leq t < 1$), respectively around a representative synapse of our tissue ball, and in the whole ball. In the absence of feedback, i.e., $F_{syn-rel} = 0$, glutamate builds up during the transient activity increase but is then quickly removed by diffusion and uptake, decreasing to pre-stimulus concentrations (black traces). In the presence of feedback instead, glutamate grows higher during and after stimulation, eventually switching to persistent toxic concentrations (red traces). That is, the positive feedback of glutamate on neural activity amplifies the initial glutamate increase by afferent stimulation, which drives a vicious cycle of hyperactivation associated with toxic glutamate accumulation (Zott and Konnerth, 2023; Lewerenz and Maher, 2015). The feedback's sigmoid nature is such that as glutamate accumulates promoting activity rates, the associated increase in synaptic release quickly grows beyond the maximum clearance capacity by diffusion and uptake, resulting in persistent glutamate accumulation. The persistent glutamate accumulation has a simple mathematical
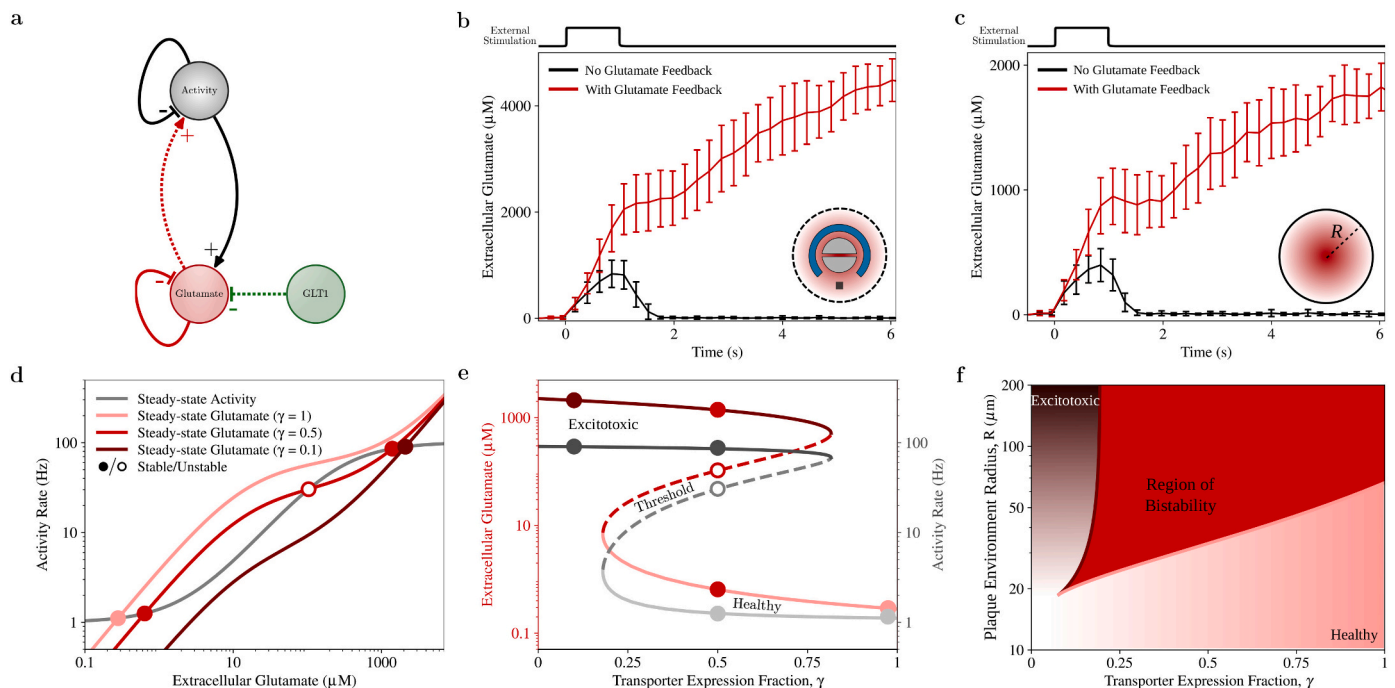

Fig. 4. Diverse conditions for excitotoxicity. **a** Model of glutamate clearance including the positive feedback of glutamate on neural activity. **b** Simulated glutamate time course in the perisynaptic space and **c** in the whole plaque microenvironment for 1 s-long activity pulse. The positive feedback of glutamate on neural activity promotes synaptic glutamate release, which can quickly exacerbate toxic glutamate build-ups. **d** Graphical analysis of the steady-state glutamate concentrations and activity rates in the plaque microenvironment reveal how healthy and excitotoxic conditions could be both plausible for intermediate astrocytic transporter expressions γ (solid red circles) in the presence of glutamate feedback on the activity. **e** Compatibly with this scenario, the bifurcation diagrams for the steady-state glutamate/activity as a function of γ reveal the existence of a region of bistable glutamate and activity levels for $0.2 < \gamma < 0.8$. **f** In such a region, the threshold of excitotoxicity nonlinearly varies with γ and radial size R of the plaque microenvironment. For colour interpretation, the reader is referred to the web version of this article.

interpretation that can be evinced from the graphical solutions of Eqs. (1) and (4) in the long-term when extracellular glutamate and neural activity reach a consistent and unchanging configuration. Fig. 4d shows these solutions by the intersection of the gray and red curves respectively for $\frac{d}{dt}\nu = 0$ and $\frac{d}{dt}g = 0$ for the three transporter expressions (γ) already considered in Fig. 3. One solution exists at low glutamate and activity rates for large transporter expression ($\gamma = 1$, pink circle), reflecting a healthy tissue state. Likewise, one solution exists in the toxic tissue state characterized by high glutamate and activity occurring for strongly reduced transporter expressions ($\gamma = 0.1$, dark red circle). However, both healthy and toxic states are viable for intermediate transporter expressions ($\gamma = 0.5$, full red circles) consistent with a scenario of bistability. In this scenario, as revealed by our simulations in Fig. 4c, we could start from the healthy state but end in toxicity as soon as activity and glutamate increase beyond levels set by the unstable solution marked by the empty red circle.

Mapping unstable and stable solutions for all possible transporter expressions results in the diagrams in Fig. 4e, technically known as bifurcation diagrams. Their characteristic 'S' shape is a hallmark of bistability (Slepchenko and Terasaki, 2004) insofar as healthy and toxic states, respectively represented by the diagrams' low (pink) and high branches (red), coexist for transporter expressions between $0.2 < \gamma < 0.8$. For such expression, the plaque microenvironment could thus become toxic or stay healthy depending on whether the local activity and glutamate levels are above or below the dashed threshold. At the same time, as far as the plaque microenvironment exists in the bistable regime, switching between healthy and toxic conditions is always possible by appropriate perturbations of activity and glutamate across the threshold. This can be therapeutically advantageous since toxicity could be reverted, thus slowing, halting, or reverting AD progression.

Because the bistability region separates between healthy-only ($\gamma > 0.8$) and toxic-only transporter expressions ($\gamma < 0.2$), we can liken it to a threshold for the transition between the two as transporter expression reduces with Aβ accumulation during preclinical AD progression. However, the nature of such a threshold is complex insofar as the emergence of bistability does not necessarily cause the transition but rather introduces the chance for it. Since this chance correlates with how far the dashed threshold in the bifurcation diagrams is with respect to the final state (Izhikevich, 2007), we conclude that the *risk* of toxicity turns into certainty when transporters reduce below $\gamma \approx 0.2$. Conversely, the *opportunity* to rescue healthy conditions increases with transporter expressions approaching the upper boundary of the bistability region, i.e., $\gamma \approx 0.8$. We want to understand when looking for bistability for diagnostics and therapeutic purposes makes sense. Since the spatial extent of Aβ accumulations controls how far toxicity develops from them (Hefendehl et al., 2016), toxic conditions could then be envisaged only for sufficiently large tissue balls. Indeed, mapping the boundaries of healthy (pink) and toxic conditions (red) in terms of the microenvironment's transporter expression and radius (R) in Fig. 4f reveals how they delimit a hashed region of bistability originating from a cusp. Below this cusp, we are looking at small tissue balls of radii $R < 20$ μm where locally-released glutamate can always diffuse out from regardless of their small transporter expression ($\gamma < 0.1$) (white shades). Hence, there is no clear separation between healthy and toxic states in such confined tissue environments because toxic glutamate concentrations can only build up by appropriate levels of exogenously maintained local activity (Supplementary Fig. 4). Conversely, as we look at larger tissue balls ($R > 20$ μm), locally released glutamate molecules need to travel longer distances to escape from it, facilitating glutamate accumulation regardless of transporter expression. This increases the chance of developing toxicity as reflected by a bistability's transporter expression range that increases with the ball's radius.

It is intriguing to correlate the growth of the bistability region with its robustness against local variations in transporter expressions (Tong

et al., 2017; Hefendehl et al., 2016; Scimemi et al., 2013) as the spatial extension of Aβ deposition increases with AD progression. Insofar as the gross of this deposition likely predates the onset of clinical AD (Jack Jr et al., 2010), we could predict that the closer to clinical manifestations we are, the more we could exploit bistability to avoid toxic developments that would exacerbate AD symptoms. In practice, however, we will have to take into account that the degree of Aβ eposition also correlates with alterations in the tissue cytoarchitecture accounted for by variations of the extracellular volume fraction (α) and the tortuosity of the diffusion pathway of glutamate (λ, Eq. (1)) (Bondareff, 2013; Syková et al., 2005). Although such variations may be variegated, they will ultimately act against the emergence of bistability for sufficiently high Aβ depositions, regardless of their underpinning molecular mechanisms (Supplementary Fig. 5).

2.4. Multiple trajectories with unique risk exist towards clinical AD syndrome

The process of Aβ accumulation preceding clinical AD is inherently dependent on intracellular Ca^{2+} and vice versa (Bezprozvanny and Mattson, 2008). Altered neuronal cytosolic Ca^{2+} accelerates Aβ formation, whereas Aβ peptides, particularly in soluble oligomeric forms, induce Ca^{2+} disruptions. This reciprocal interaction results in a feed-forward cycle of toxic Aβ generation and Ca^{2+} perturbations, which can exacerbate AD pathology (Demuro et al., 2010). Moreover, another feed-forward cycle exists between Ca^{2+} and neural activity. Ongoing activity modulates intraneuronal Ca^{2+} levels (Higley and Sabatini, 2012), while in turn Ca^{2+} crucially regulates glutamate release from synaptic terminals (Schneggenburger and Neher, 2005). In this way, the Ca^{2+}-dependent Aβ accumulation becomes inherently activity-dependent, and so does astrocytic transporter expression. How could the combination of these pathways influence the onset of hyperactivity in prodromal AD? The sigmoid laws governing the bistability of the glutamate vicious cycle on activity as a function of transporter expression (Fig. 4) also account for bistability as a function of the tissue baseline activity (ν_0) (Fig. 5a,b) which is known to increase with AD emergence (Zott and Konnerth, 2023). In particular, our tissue model predicts the existence of a threshold of glutamatergic activity (dashed lines in Fig. 5b.2) for basal activity rates up to about 15 Hz. Below this rate, it will always be possible to rescue the healthy state starting from excitotoxic conditions by perturbations of initial conditions below that threshold. Conversely, as soon as basal activity increases beyond 15 Hz, excitotoxicity becomes practically unavoidable (Fig. 5b.3). A similar scenario of bistability also occurs for Ca^{2+}-dependent Aβ accumulation (De Caluwé and Dupont, 2013, and Supplementary Fig. 6). The process can indeed be described by sigmoid laws akin to those governing the glutamate/activity vicious cycle (Appendix D), predicting that low vs. high Aβ and Ca^{2+} concentrations coexist for the same basal activity rate up to about 50 Hz (Fig. 5d).

The combination of the bistability scenarios of the two processes would account, at least in principle, for four possible tissue states: a healthy state characterized by low extracellular glutamate and local activity with low Aβ and Ca^{2+} levels, a pathogenic state where excitotoxicity coexists with high Aβ and Ca^{2+} concentrations, and two other "mixed" states where low glutamate/activity (respectively low Aβ/ Ca^{2+}) combine with high Aβ and Ca^{2+} (respectively, high glutamate and activity rates). However, because sigmoid laws govern how Ca^{2+} regulate synaptic glutamate release (Schneggenburger and Neher, 2005), and how Aβ could reduce glutamate uptake by astrocytic transporters (Fig. 5e) (Fernández-Tomé et al., 2004, and Appendix D) we should expect a nonuniform distribution for the probability of occurrence of one state vs. another. We thus set to characterize the admissible states in AD emergence by including in our model of glutamate-mediated hyperactivity an effective description of Ca^{2+} dependent Aβ build-up (De Caluwé and Dupont, 2013, and Appendix D) and considering two
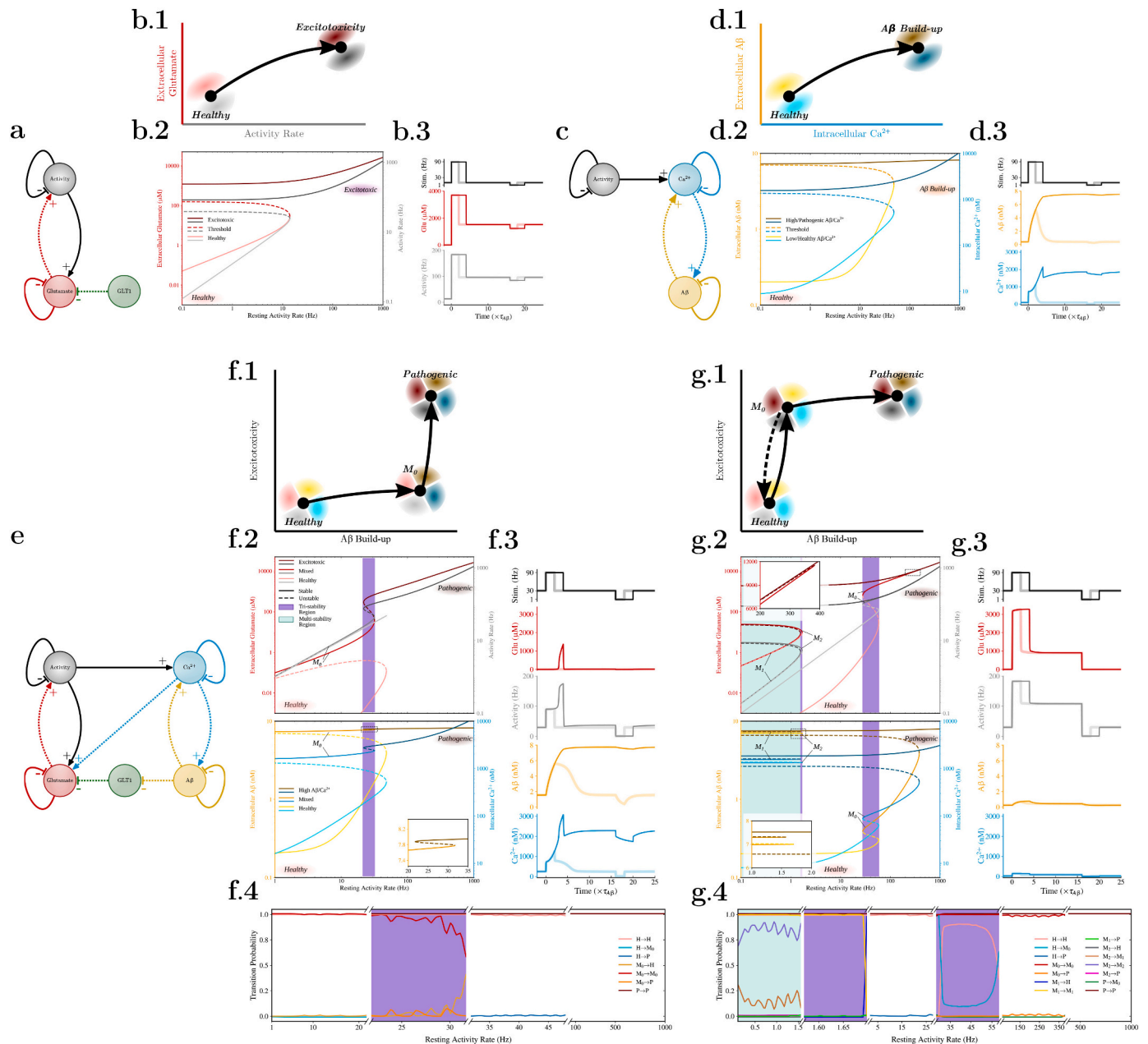
Fig. 5. Different trajectories for AD emergence. Two activity-dependent feed-forward processes exist in Aβ pathogenesis respectively by **a,b** the glutamate-mediated vicious cycle on activity, and **c,d** the Ca^{2+}-dependent vicious cycle on Aβ build-up. **b.2,c.2** Both cycles can mediate a scenario of bistability for basal activity rates with **b.3,c.3** irreversible pathogenic states. **e** The two cycles are also coupled by nonlinear Ca^{2+}-dependent glutamate release and nonlinear Aβ-reduction of transporter uptake, accounting for multiple scenarios of AD emergence, depending on the biophysical properties of affected neural circuits. **f** In one scenario, Aβ predates excitotoxicity, whereas in another **g** excitotoxicity may anticipate Aβ build-ups. These different scenarios are possible by intermediate states manifesting only some pathological features (e.g., excitotoxic conditions vs. Aβ/Ca^{2+} build-ups), which can account for multiple nuances of pathogenic tissue in AD progression beyond simple distinction between healthy vs. pathological. **f.4,g.4** Probabilities of permissible transitions between states in the function of the basal activity rate (ν_0). The probability of transition between two states *A* and *B*, i.e., *A→B*, is computed following Kaszás et al. (2019) by the area ratio between the set of all initial conditions that from *A* ends in *B* for an increment $\nu_0 \rightarrow \nu_0 + \Delta$, divided by the set of initial conditions ending in *B* before such increment.

different scenarios of Ca^{2+} affinity of synaptic release (K_R) and activity-dependent Ca^{2+} signaling (η_C) that could be representative of the heterogeneity of cortical synaptic circuits (van Oostrum et al., 2023; Wang and Dudko, 2021; Zhu et al., 2018, and Appendix F).

Fig. 5f considers the case of synaptic circuits characterized by a moderate Ca^{2+} affinity ($K_R = 3.6$ μM) and an equally moderate activity-dependent Ca^{2+} production ($\eta_C = 1$ s). Our model predicts that healthy vs. pathogenic states in such circuits are separated by an intermediate one (M_0) characterized by extracellular glutamate levels and activity rates close to healthy conditions while Aβ and Ca^{2+} concentrations

approach pathogenic ones (Fig. 5f.2). In this case, an increase in the local basal activity that results in excitotoxic pathogenic conditions could only be partially mitigated by any treatment to reduce basal activity. Reducing basal activity in such pathogenic conditions only rescues glutamatergic activity levels attained in healthy conditions, but not Aβ/Ca^{2+} ones (solid dark traces in Fig. 5f.3). Thus, in agreement with the Aβ cascade hypothesis of AD (Selkoe and Hardy, 2016), this scenario predicts that Aβ build-up predates the onset of excitotoxicity.

The opposite scenario is instead observed in Fig. 5g, which considers the case of a sample tissue whose local circuits could display increased

synaptic release ($K_R = 80$ nM) but weaker activity-dependent Ca^{2+} production ($\eta_C = 0.1$ s). The bifurcation diagrams associated with this case reveal instead the existence of an intermediate state M_0 where high glutamate/activity rates coexist with low $A\beta/Ca^{2+}$ levels (Fig. 5g.2). This suggests that such circuits appear more likely to develop excitotoxic conditions, as reflected by the robust glutamate and activity surge against a mild increase in $A\beta/Ca^{2+}$ for the increase in basal activity that in the previous scenario was, on the contrary, primarily amyloidogenic. Moreover, it may be noted how reverting such an increase could revert both excitotoxic conditions and $A\beta$ and Ca^{2+} build-ups, ultimately rescuing healthy conditions (Fig. 5g.3).

A closer look at the bifurcation diagrams associated with the two tissue scenarios pinpoints the origin of such reversibility to the domain of existence of the diagram branch associated with the intermediate M_0 state and how it is positioned between the healthy and pathogenic ones. In Fig. 5f.2, the M_0 branch exists for all basal activity rates up to the right boundary of the purple area, which occurs before the healthy branch's termination. Moreover, the M_0 and pathogenic branches together span the whole range of permissible basal activity rates, making rescuing healthy conditions impossible from either state by the sole reduction of the basal activity. Conversely, in Fig. 5g.2, the M_0 branch only exists in a confined range of basal activity values, originating around 25 Hz and extending beyond the healthy branch's upper limit, up to roughly 450 Hz. In this way, any basal activity reduction below the purple-shaded area's lower boundary could rescue healthy conditions.

The existence of "mixed" tissue states accounting for excitotoxicity but not $A\beta/Ca^{2+}$ build up, or vice versa, is robust for a broad range of biophysical tissue parameters (Supplementary Fig. 8). At the same time, different biophysical properties could account for even more complex scenarios where more than one intermediate state exists between healthy and pathogenic (Supplementary Fig. 9). For example, the bifurcation diagrams in Fig. 5g.2 also reveal that two additional states, M_1 and M_2, account for similar $A\beta/Ca^{2+}$ build-ups but different intermediate levels of extracellular glutamate accumulation and associated activity at low basal activity rates (<1.5 Hz). An analysis of the permissible transitions allowed from/to these states (Fig. 5g.4) then hints that transient increases of basal activity could be sufficient to destabilize such states (e.g., $M_1, M_2 \rightarrow H$), making the tissue fall back to somehow healthier conditions of lower glutamatergic activity and $A\beta$ burden.

The chance to end in one of such intermediate states during AD emergence will ultimately depend on the initial state of the tissue. This is because the set of initial values of extracellular glutamate and $A\beta$ concentrations, intracellular Ca^{2+}, and local activity rates that determine whether the tissue ends up in one state or another change with the basal rate of activity (Figs. 5f.4 and 5g.4). Thus, as the basal rate changes with the AD emergence, so does the probability of transitioning from healthy to intermediate states before ending into pathological ones. Since the tissue's biophysical properties will ultimately dictate how this transition probability changes, we conclude that the risk of developing excitotoxicity vs. $A\beta/Ca^{2+}$ build-ups in AD is variegated throughout the brain, with different sites expected to develop only some aspects of the pathology rather than others.

3. Discussion

We presented a mathematical model of $A\beta$-dependent neuronal hyperactivation as an early-stage hallmark of neuronal dysfunction in Alzheimer's disease (AD) (Zott et al., 2019; Busche et al., 2012; Busche et al., 2008). The model replicates the experimental observation that extracellular $A\beta$ leads to the impairment of glutamate uptake by astrocytic transporters, resulting in the accumulation of perisynaptic glutamate. In turn, the excessive extracellular glutamate increases the activity levels further, mimicking neuronal depolarization by glutamate binding to ionotropic glutamate receptors, potentially creating a vicious cycle that initiates and sustains hyperactivity (Zott and Konnerth, 2023;

Busche and Konnerth, 2016). In analogy with experimental observations, this vicious cycle depends on the baseline neuronal activity (Zott et al., 2019). Neurons affected by the $A\beta$-dependent reduction of glutamate uptake can experience a buildup of glutamate levels, perpetuating hyperactivity. In contrast, inactive neurons with low levels of glutamatergic stimulation are less likely to become part of this harmful cycle.

Although we developed our model with the microenvironment in the proximity of $A\beta$ plaques in mind, the model can also be adapted for studying the emergence of toxicity in the extracellular space at some distance from plaques. This is because we do not explicitly model the process of $A\beta$ deposition and plaque formation but rather take them into account as a source of extracellular accumulations of soluble $A\beta$ oligomers (Hefendehl et al., 2016; Grienberger et al., 2012; Condello et al., 2011). Additionally, we refrain from detailing the source of soluble $A\beta$ that is independent of Ca^{2+} and activity to consider the possibility that besides plaques, soluble $A\beta$ oligomers could also originate from glial cells and other yet-to-be-discovered sources in the tissue (Viola and Klein, 2015; Veeraraghavalu et al., 2014; Skaper et al., 2009). In this framework, we embrace the emerging notion that more than $A\beta$ deposition per se, which only weakly correlates with cognitive impairment in sporadic AD, soluble $A\beta$ oligomer accumulation, which predates plaque formation, could be an earlier trigger of the disease (Walsh and Selkoe, 2020; Viola and Klein, 2015).

3.1.1. Multiple trajectories to AD pathology originate from the vicious cycle of $A\beta$ -mediated hyperactivity

An important prediction of our model is that the interaction of glutamatergic activity with intracellular Ca^{2+} and $A\beta$ production makes the onset of $A\beta$-dependent hyperactivation conditions inherently variegated. Neural hyperactivity generally positively correlates with $A\beta$ levels and vice versa, mirroring experimental findings (Bero et al., 2011; Cirrito et al., 2005; Kamenetz et al., 2003). However, we also reveal that potentially excitotoxic hyperactivity and pathogenic $A\beta$ buildups could be attained independently for distinct baseline neuronal activities, depending on the tissue's biophysical properties. In other words, inherent differences in brain regions' cytoarchitecture and molecular organization could account for different mechanisms of AD emergence, eventually reflecting on the heterogeneity of the disease at later, more advanced syndromic stages (Ten Kate et al., 2018; Zhang et al., 2016).

AD's regional specificity almost certainly correlates with dynamical heterogeneity (Habes et al., 2020). Effectively, our model predicts that different tissue biophysical properties could result in different trajectories for AD emergence, where either hyperactivity predates $A\beta$ deposition or vice versa. Moreover, both scenarios could be subjected to hysteresis, whereby the effect of a perturbation of baseline activity would generally vary with the AD progression stage. This supports the notion that AD etiology is complex, and the disease encompasses a spectrum of subtypes that could conveniently be stratified by region and stage (Young et al., 2018).

Our prediction that AD progression could be characterized by various mixed states where excitotoxicity emerges before $A\beta$ accumulation, and vice versa, corroborates the idea of a continuum of AD pathology (Jack Jr et al., 2013; Jack Jr et al., 2010). At the same time, it also challenges our notion of a single preclinical stage of the disease in favor of multiple scenarios of AD emergence, each possibly characterized by a unique risk (Frisoni et al., 2022). In this framework, the fact that hyperactivity stemming from astrocyte glutamatergic dysfunction could predate $A\beta$ accumulation is a promising avenue for biomarker development in the asymptomatic phase of the disease (Carter et al., 2019; Sperling et al., 2011). On the other hand, we also argue that, in light of the complex nonlinear nature of the interactions between excitotoxicity and $A\beta/Ca^{2+}$ accumulations, the synergy between $A\beta$

deposition and hyperactivity, rather than their additive effects, is likely a better predictor of AD emergence, as it is the case, for example, of considering Aβ plaques and tau tangles together in diagnostics of later stages of the disease (Pascoal et al., 2017).

3.1.2. Beyond the vicious cycle of Aβ-mediated hyperactivity

A critical clinical observation is that pathologically disrupted neural circuits in AD present a dynamic disequilibrium in the E/I balance (Zott and Konnerth, 2023; Targa Dias Anastacio et al., 2022; Palop and Mucke, 2010). This imbalance manifests biphasically, displaying hyperactivity during asymptomatic stages and transitioning to hypoactivity in later phases of the disease (Busche and Konnerth, 2016; Alexander et al., 2002). Consistent with these insights, AD patients exhibit an augmented predisposition to seizures at earlier disease stages, followed by a subsequent attenuation of seizure risk (Vossel et al., 2013). Our model aligns with these clinical observations and posits that a vicious cycle of Aβ-mediated glutamate accumulation may mediate the hyperactive phase. Simultaneously, it underscores the need to explore alternative processes possibly linked with tau deposition to curtail this hyperactivity (Harris et al., 2020).

An open question in the field pertains to explaining the somewhat elevated seizure risk observed with hypoactivity in the later disease stages (Harris et al., 2020; Vossel et al., 2013; Palop and Mucke, 2016). Our model introduces a plausible explanation, suggesting that the hypoactive phase might correspond to intermediate states of hyperactivity. Within this framework, local neural populations could remain hyperexcitable despite ensemble activity rates that do not meet the criteria for epileptiform classification (Vossel et al., 2017). At the same time, the existence of these populations in an intermediate state of excitability positions them closer to the threshold for triggering epileptiform activity at the macroscopic level through the synergistic interaction with other populations (Chameh et al., 2023). This agrees with the often-observed multifocal nature of AD-related seizures (Vossel et al., 2017) and calls for future theoretical and experimental investigations focusing on unraveling the correlations between local gradients in Aβ and tau deposition and potential epileptic foci at the microcircuit level (Harris et al., 2020).

The nonlinearity of the molecular biology underpinning AD pathology remains to be fully characterized. Future extensions of our model should also consider the possibility of direct coupling of activity with Aβ production through endosomal and ectoenzymatic pathways (Gallego Villarejo et al., 2022; Guan et al., 2021). Additionally, the direct modulation of GLT1 expression by Ca^{2+}-dependent pathways, in addition to Aβ, should be considered (Todd and Hardingham, 2020; Stargardt et al., 2015). Another consideration is that neuronal transporters, rather than astrocytic transporters, could be the primary mechanism for glutamate uptake in specific synaptic circuits (Rimmele et al., 2021; Petr et al., 2015). Furthermore, it is worth exploring the idea that Aβ-mediated oxidative stress and gliosis could modify GLT1 expression by altering the astrocytic cytoskeleton (Carter et al., 2019; Wyssenbach et al., 2016; Alberdi et al., 2013). Ultimately, there is a chance that astrocytic GLT1 could modulate the E/I balance by regulating neurotransmitter resources in both glutamatergic and GABAergic networks (Hertz, 2013). The nonlinearity of these pathways and many possible others behind AD molecular pathophysiology (Henstridge et al., 2019) will only enrich the mosaics of potential tissue states in AD emergence (Latulippe et al., 2018), and, thus, the putative trajectories for the disease's onset. Since the combination of the different nonlinearities uniquely characterizes the risk of each trajectory, interpreted as the chance for their occurrence, it also opens unforeseen avenues for personalized treatment by risk reduction interventions informed by the inherent nonlinear nature of the underpinning reactome (Frisoni et al., 2022; Frisoni et al., 2020).

3.1.3. Diagnostic, prognostic, and treatment opportunities

In the pursuit of effective AD theranostics, a pivotal question is what factors or circumstances dictate that specific neuronal cells and brain regions succumb to catastrophic outcomes when burdened by excitotoxic Aβ lesions, while others exhibit a higher threshold of withstanding toxicity, preserving their normal function (Mrdjen et al., 2019). Existing strategies employ a combination of diverse biomarker readouts, imaging techniques, and clinical data to anticipate the risk of developing AD symptoms (Chen et al., 2021; Wang et al., 2021; Huang et al., 2020). Each identified risk factor is quantified on an incremental scale, and their weighted sum relative to other factors estimates pathological risk. A critical challenge in this context is to precisely assess the contribution of each factor, considering the potential dynamic evolution of its impact on pathology throughout the progression of the disease (Jack Jr et al., 2013; Sperling et al., 2011). This study introduces a modeling framework designed to address this challenge, offering a mathematical characterization of the rules governing the intricate interplay between intrinsic and extrinsic properties influencing regional and cellular vulnerability to Aβ-mediated hyperactivity in the onset of AD.

As we quantify intermediate mixed states through where individual AD pathogenic features may develop independently, we also argue that characterizing the variety of those states is only possible by the simultaneous measurements of extracellular Aβ and glutamate levels, along with markers of tissue activation such as neuronal firing rate and intracellular Ca^{2+}. At the same time, the possibility that those mixed states may be not only transitional to the pathology but also accessible from more severe conditions in the pathology progression presents potential opportunities for therapeutic intervention. The subsequent challenge involves identifying clinical and pharmacological tools that can modify specific aspects of Aβ-mediated hyperactivity. This modification, captured by variations in our model parameters, could potentially provide patients with access to the remission of pathological features and redirect the disease trajectory towards a more favorable outcome.

Because Aβ may also mediate hyperactivity by weakening GABAergic synaptic circuits (Harris et al., 2020; Giovannetti and Fuhrmann, 2019; Palop and Mucke, 2016) or by blood-brain barrier disruptions (Hickman et al., 2023; Sweeney et al., 2018), our model necessitates future extensions to clarify how these pathways, either individually or in conjunction with the vicious cycle of Aβ-mediated excitotoxicity, contribute to shaping the landscape of distinct AD pathological states and their associated risks. Recent strides in generative artificial intelligence hold promise in the classification and prediction of diverse states and therapeutic entry points in AD theranostics (Winchester et al., 2023; Fabrizio et al., 2021). However, their effectiveness is limited by the finite nature of the datasets informing them and the interpretability of their predictions (Winchester et al., 2023; de la Fuente Garcia et al., 2020). In this context, our modeling approach serves as a valuable complement in diagnosic validation and refinement by bridging gaps in data discretization by leveraging biophysical laws governing the reactome to capture the continuum of the AD spectrum (Aisen et al., 2017). The further adaptability of our approach to characterize aspects of AD molecular pathophysiology at single synapses and synaptic and tissue ball levels can ultimately provide unmatched insights into the molecular mechanisms of the disease's etiology. We recognize in the ability to bridge across brain levels, linking micro- with macroscopic molecular and cellular circuits underpinning AD, the ultimate advantage of biophysical modeling against machine-learning approaches to unveil compensatory biophysical mechanisms to bolster resilience against an individual's risk of developing the disease.

4. Materials and methods

The detailed derivation of the models presented in this study, the exposition of the numerical methods adopted for their simulation and analysis, and the estimation of the models' biophysical parameters may be found in the Appendices to this study in the Supplementary Information available online through the *Neurobiology of Disease*'s page for this article.

Funding

Credit authorship contribution statement

Giulio Bonifazi: Writing – review & editing, Writing – original draft, Validation, Software, Methodology, Investigation, Formal analysis, Data curation, Conceptualization. **Celia Luchena:** Writing – review & editing, Validation. **Adhara Gaminde-Blasco:** Writing – review & editing, Validation. **Carolina Ortiz-Sanz:** Writing – review & editing, Validation. **Estibaliz Capetillo-Zarate:** Writing – review & editing, Validation. **Carlos Matute:** Writing – review & editing, Validation, Conceptualization. **Elena Alberdi:** Writing – review & editing, Validation, Conceptualization. **Maurizio De Pittà:** Writing – review & editing, Writing – original draft, Validation, Supervision, Software, Methodology, Investigation, Formal analysis, Data curation, Conceptualization.

Declaration of competing interest

The authors declare no competing interests in the pursuit of this study.

Appendix. Supplementary data

Supplementary Material including all the Appendices for this article can be found online at https://doi.org/10.1016/j.nbd.2024.106473.

References

Aisen, P.S., Cummings, J., Jack, C.R., Morris, J.C., Sperling, R., Frölich, L., Jones, R.W., Dowsett, S.A., Matthews, B.R., Raskin, J., et al., 2017. On the path to 2025: understanding the Alzheimer's disease continuum. Alzheimers Res. Ther. 9, 1–10.

Alberdi, E., Wyssenbach, A., Alberdi, M., Sánchez-Gómez, M.V., Cavaliere, F., Rodríguez, J.J., Verkhratsky, A., Matute, C., 2013. Ca^{2+}-dependent endoplasmic reticulum stress correlates with astrogliosis in oligomeric amyloid β-treated astrocytes and in a model of Alzheimer's disease. Aging Cell 12, 292–302.

Alexander, G.E., Chen, K., Pietrini, P., Rapoport, S.I., Reiman, E.M., 2002. Longitudinal PET evaluation of cerebral metabolic decline in dementia: a potential outcome measure in Alzheimer's disease treatment studies. Am. J. Psychiatry 159, 738–745.

Bakker, A., Krauss, G.L., Albert, M.S., Speck, C.L., Jones, L.R., Stark, C.E., Yassa, M.A., Bassett, S.S., Shelton, A.L., Gallagher, M., 2012. Reduction of hippocampal hyperactivity improves cognition in amnestic mild cognitive impairment. Neuron 74, 467–474.

Bakker, A., Albert, M.S., Krauss, G., Speck, C.L., Gallagher, M., 2015. Response of the medial temporal lobe network in amnestic mild cognitive impairment to therapeutic intervention assessed by fMRI and memory task performance. NeuroImage: Clin. 7, 688–698.

Barbour, B., 2001. An evaluation of synapse independence. J. Neurosci. 21, 7969–7984.

Bass, B., Upson, S., Roy, K., Montgomery, E.L., Jalonen, T.O., Murray, I.V., 2015. Glycogen and amyloid-beta: key players in the shift from neuronal hyperactivity to hypoactivity observed in Alzheimer's disease? Neural Regen. Res. 10, 1023.

Bergles, D.E., Jahr, C.E., 1998. Glial contribution to glutamate uptake at schaffer collateral–commissural synapses in the hippocampus. J. Neurosci. 18, 7709–7716.

Bergles, D.E., Diamond, J.S., Jahr, C.E., 1999. Clearance of glutamate inside the synapse and beyond. Curr. Opin. Neurobiol. 9, 293–298.

Bero, A.W., Yan, P., Roh, J.H., Cirrito, J.R., Stewart, F.R., Raichle, M.E., Lee, J.M., Holtzman, D.M., 2011. Neuronal activity regulates the regional vulnerability to amyloid-β deposition. Nat. Neurosci. 14, 750–756.

Bezprozvanny, I., Mattson, M.P., 2008. Neuronal calcium mishandling and the pathogenesis of Alzheimer's disease. Trends Neurosci. 31, 454–463.

Blennow, K., Zetterberg, H., 2018. Biomarkers for Alzheimer's disease: current status and prospects for the future. J. Intern. Med. 284, 643–663.

Bondareff, W., 2013. Age-related changes in brain extracellular space affect processing of amyloid-β peptides in Alzheimer's disease. J. Alzheimers Dis. 35, 1–6.

Bookheimer, S.Y., Strojwas, M.H., Cohen, M.S., Saunders, A.M., Pericak-Vance, M.A., Mazziotta, J.C., Small, G.W., 2000. Patterns of brain activation in people at risk for Alzheimer's disease. N. Engl. J. Med. 343, 450–456.

Busche, M.A., Konnerth, A., 2016. Impairments of neural circuit function in Alzheimer's disease. Philos. Trans. R. Soc. B 371, 20150429.

Busche, M.A., Eichhoff, G., Adelsberger, H., Abramowski, D., Wiederhold, K.H., Haass, C., Staufenbiel, M., Konnerth, A., Garaschuk, O., 2008. Clusters of hyperactive neurons near amyloid plaques in a mouse model of Alzheimer's disease. Science 321, 1686–1689.

Busche, M.A., Chen, X., Henning, H.A., Reichwald, J., Staufenbiel, M., Sakmann, B., Konnerth, A., 2012. Critical role of soluble amyloid-β for early hippocampal hyperactivity in a mouse model of Alzheimer's disease. Proc. Natl. Acad. Sci. 109, 8740–8745.

Buzsaki, G., 2006. Rhythms of the Brain. Oxford University Press.

Carter, S.F., Herholz, K., Rosa-Neto, P., Pellerin, L., Nordberg, A., Zimmer, E.R., 2019. Astrocyte biomarkers in Alzheimer's disease. Trends Mol. Med. 25, 77–95.

Cavelier, P., Attwell, D., 2005. Tonic release of glutamate by a DIDS-sensitive mechanism in rat hippocampal slices. J. Physiol. 564, 397–410.

Chameh, H.M., Falby, M., Movahed, M., Arbabi, K., Rich, S., Zhang, L., Lefebvre, J., Tripathy, S.J., De Pittà, M., Valiante, T.A., 2023. Distinctive biophysical features of human cell-types: insights from studies of neurosurgically resected brain tissue. Front. Synapt. Neurosci. 15, 1250834.

Chen, W., Li, S., Ma, Y., Lv, S., Wu, F., Du, J., Wu, H., Wang, S., Zhao, Q., 2021. A simple nomogram prediction model to identify relatively young patients with mild cognitive impairment who may progress to Alzheimer's disease. J. Clin. Neurosci. 91, 62–68.

Cirrito, J.R., Yamada, K.A., Finn, M.B., Sloviter, R.S., Bales, K.R., May, P.C., Schoepp, D. D., Paul, S.M., Mennerick, S., Holtzman, D.M., 2005. Synaptic activity regulates interstitial fluid amyloid-β levels in vivo. Neuron 48, 913–922.

Clements, J.D., Lester, R.A.J., Tong, G., Jahr, C.E., Westbrook, G.L., 1992. The time course of glutamate in the synaptic cleft. Science 258, 1498–1501.

Condello, C., Schain, A., Grutzendler, J., 2011. Multicolor time-stamp reveals the dynamics and toxicity of amyloid deposition. Sci. Rep. 1, 19.

Curran, O.E., Qiu, Z., Smith, C., Grant, S.G., 2021. A single-synapse resolution survey of PSD95-positive synapses in twenty human brain regions. Eur. J. Neurosci. 54, 6864–6881.

Danbolt, N.C., 2001. Glutamate uptake. Prog. Neurobiol. 65, 1–105.

Danbolt, N.C., Furness, D.N., Zhou, Y., 2016. Neuronal vs glial glutamate uptake: resolving the conundrum. Neurochem. Int. 98, 29–45.

De Caluwé, J., Dupont, G., 2013. The progression towards alzheimer's disease described as a bistable switch arising from the positive loop between amyloids and Ca2+. J. Theor. Biol. 331, 12–18.

de la Fuente Garcia, S., Ritchie, C.W., Luz, S., 2020. Artificial intelligence, speech, and language processing approaches to monitoring Alzheimer's disease: a systematic review. J. Alzheimers Dis. 78, 1547–1574.

Demuro, A., Parker, I., Stutzmann, G.E., 2010. Calcium signaling and amyloid toxicity in Alzheimer disease. J. Biol. Chem. 285, 12463–12468.

Dickerson, B., Salat, D., Greve, D., Chua, E., Rand-Giovannetti, E., Rentz, D., Bertram, L., Mullin, K., Tanzi, R., Blacker, D., et al., 2005. Increased hippocampal activation in mild cognitive impairment compared to normal aging and AD. Neurology 65, 404–411.

Fabrizio, C., Termine, A., Caltagirone, C., Sancesario, G., 2021. Artificial intelligence for Alzheimer's disease: promise or challenge? Diagnostics 11, 1473.

Fernández-Tomé, P., Brera, B., Arévalo, M.A., de Ceballos, M.L., 2004. β-amyloid$_{25-35}$ inhibits glutamate uptake in cultured neurons and astrocytes: modulation of uptake as a survival mechanism. Neurobiol. Dis. 15, 580–589.

Frere, S., Slutsky, I., 2018. Alzheimer's disease: from firing instability to homeostasis network collapse. Neuron 97, 32–58.

Frey, C.H., Sumeet, R.P., 2002. Identification and review of sensitivity analysis methods [interaktyvus], [žiūrėta 2010-03-14]. Risk Anal. 22, 553–578.

Fries, P., Nikolić, D., Singer, W., 2007. The gamma cycle. Trends Neurosci. 30, 309–316.

Frisoni, G.B., Molinuevo, J.L., Altomare, D., Carrera, E., Barkhof, F., Berkhof, J., Delrieu, J., Dubois, B., Kivipelto, M., Nordberg, A., et al., 2020. Precision prevention of Alzheimer's and other dementias: anticipating future needs in the control of risk factors and implementation of disease-modifying therapies. Alzheimers Dement. 16, 1457–1468.

Frisoni, G.B., Altomare, D., Thal, D.R., Ribaldi, F., van der Kant, R., Ossenkoppele, R., Blennow, K., Cummings, J., van Duijn, C., Nilsson, P.M., et al., 2022. The probabilistic model of Alzheimer disease: the amyloid hypothesis revised. Nat. Rev. Neurosci. 23, 53–66.

Gallego Villarejo, L., Bachmann, L., Marks, D., Brachthäuser, M., Geidies, A., Müller, T., 2022. Role of intracellular amyloid β as pathway modulator, biomarker, and therapy target. Int. J. Mol. Sci. 23, 4656.

Giovannetti, E.A., Fuhrmann, M., 2019. Unsupervised excitation: GABAergic dysfunctions in Alzheimer's disease. Brain Res. 1707, 216–226.

Grienberger, C., Rochefort, N.L., Adelsberger, H., Henning, H.A., Hill, D.N., Reichwald, J., Staufenbiel, M., Konnerth, A., 2012. Staged decline of neuronal function in vivo in an animal model of Alzheimer's disease. Nat. Commun. 3, 774.

Guan, P.P., Cao, L.L., Wang, P., 2021. Elevating the levels of calcium ions exacerbate Alzheimer's disease via inducing the production and aggregation of β-amyloid protein and phosphorylated tau. Int. J. Mol. Sci. 22, 5900.

Habes, M., Grothe, M.J., Tunc, B., McMillan, C., Wolk, D.A., Davatzikos, C., 2020. Disentangling heterogeneity in Alzheimer's disease and related dementias using data-driven methods. Biol. Psychiatry 88, 70–82.

Harris, S.S., Wolf, F., De Strooper, B., Busche, M.A., 2020. Tipping the scales: peptide-dependent dysregulation of neural circuit dynamics in Alzheimer's disease. Neuron 107, 417–435.

Hefendehl, J.K., Wegenast-Braun, B.M., Liebig, C., Eicke, D., Milford, D., Calhoun, M.E., Kohsaka, S., Eichner, M., Jucker, M., 2011. Long-term in vivo imaging of β-amyloid plaque appearance and growth in a mouse model of cerebral β-amyloidosis. J. Neurosci. 31, 624–629.

Hefendehl, J., LeDue, J., Ko, R., Mahler, J., Murphy, T., MacVicar, B., 2016. Mapping synaptic glutamate transporter dysfunction in vivo to regions surrounding aβ plaques by iglusnfr two-photon imaging. Nat. Commun. 7, 1–13.

Henstridge, C.M., Hyman, B.T., Spires-Jones, T.L., 2019. Beyond the neuron–cellular interactions early in Alzheimer disease pathogenesis. Nat. Rev. Neurosci. 20, 94–108.

Herman, M.A., Jahr, C.E., 2007. Extracellular glutamate concentration in hippocampal slice. J. Neurosci. 27, 9736–9741.

Hertz, L., 2013. The glutamate–glutamine (GABA) cycle: importance of late postnatal development and potential reciprocal interactions between biosynthesis and degradation. Front. Endocrinol. 4, 51460.

Hickman, L.B., Stern, J.M., Silverman, D.H., Salamon, N., Vossel, K., 2023. Clinical, imaging, and biomarker evidence of amyloid-and tau-related neurodegeneration in lateonset epilepsy of unknown etiology. Front. Neurol. 14, 1241638.

Higley, M.J., Sabatini, B.L., 2012. Calcium signaling in dendritic spines. Cold Spring Harb. Perspect. Biol. 4, a005686.

Hong, S., Quintero-Monzon, O., Ostaszewski, B.L., Podlisny, D.R., Cavanaugh, W.T., Yang, T., Holtzman, D.M., Cirrito, J.R., Selkoe, D.J., 2011. Dynamic analysis of amyloid β-protein in behaving mice reveals opposing changes in ISF versus parenchymal aβ during age-related plaque formation. J. Neurosci. 31, 15861–15869.

Huang, K., Lin, Y., Yang, L., Wang, Y., Cai, S., Pang, L., Wu, X., Huang, L., Initiative, A.D. N., 2020. A multipredictor model to predict the conversion of mild cognitive impairment to Alzheimer's disease by using a predictive nomogram. Neuropsychopharmacology 45, 358–366.

Huijbers, W., Mormino, E.C., Schultz, A.P., Wigman, S., Ward, A.M., Larvie, M., Amariglio, R.E., Marshall, G.A., Rentz, D.M., Johnson, K.A., et al., 2015. Amyloid-β deposition in mild cognitive impairment is associated with increased hippocampal activity, atrophy and clinical progression. Brain 138, 1023–1035.

Izhikevich, E.M., 2007. Dynamical Systems in Neuroscience: The Geometry of Excitability and Bursting. The MIT Press.

Jack Jr., C.R., Lowe, V.J., Weigand, S.D., Wiste, H.J., Senjem, M.L., Knopman, D.S., Shiung, M.M., Gunter, J.L., Boeve, B.F., Kemp, B.J., et al., 2009. Serial PIB and MRI in normal, mild cognitive impairment and Alzheimer's disease: implications for sequence of pathological events in Alzheimer's disease. Brain 132, 1355–1365.

Jack Jr., C.R., Knopman, D.S., Jagust, W.J., Shaw, L.M., Aisen, P.S., Weiner, M.W., Petersen, R.C., Trojanowski, J.Q., 2010. Hypothetical model of dynamic biomarkers of the Alzheimer's pathological cascade. Lancet Neurol. 9, 119–128.

Jack Jr., C.R., Albert, M.S., Knopman, D.S., McKhann, G.M., Sperling, R.A., Carrillo, M. C., Thies, B., Phelps, C.H., 2011. Introduction to the recommendations from the National Institute on Aging-Alzheimer's Association workgroups on diagnostic guidelines for Alzheimer's disease. Alzheimers Dement. 7, 257–262.

Jack Jr., C.R., Knopman, D.S., Jagust, W.J., Petersen, R.C., Weiner, M.W., Aisen, P.S., Shaw, L.M., Vemuri, P., Wiste, H.J., Weigand, S.D., et al., 2013. Tracking pathophysiological processes in Alzheimer's disease: an updated hypothetical model of dynamic biomarkers. Lancet Neurol. 12, 207–216.

Jagust, W., 2018. Imaging the evolution and pathophysiology of Alzheimer disease. Nat. Rev. Neurosci. 19, 687–700.

Kamenetz, F., Tomita, T., Hsieh, H., Seabrook, G., Borchelt, D., Iwatsubo, T., Sisodia, S., Malinow, R., 2003. APP processing and synaptic function. Neuron 37, 925–937.

Kasthuri, N., Hayworth, K., Berger, D.R., Schalek, R.L., Conchello, J.A., Knowles-Barley, S., Lee, D., VÃ¡zquez-Reina, A., Kaynig, V., Jones, T.R., Roberts, M., Lyskowski, J.M., Tapia, J.C., Seung, H.S., Roncal, W.G., Vogelstein, J.T., Burns, R., Sussman, D.L., Priebe, C.E., Pfister, H., Lichtman, J.W., 2015. Saturated reconstruction of a volume of neocortex. Cell 162, 648–661.

Kaszás, B., Feudel, U., Tél, T., 2019. Tipping phenomena in typical dynamical systems subjected to parameter drift. Sci. Rep. 9, 8654.

Kelley, A.S., McGarry, K., Gorges, R., Skinner, J.S., 2015. The burden of health care costs for patients with dementia in the last 5 years of life. Ann. Intern. Med. 163, 729–736.

Keskin, A.D., Kekuš, M. Adelsberger, H., Neumann, U., Shimshek, D.R., Song, B., Zott, B., Peng, T., Förstl, H., Staufenbiel, M., et al., 2017. BACE inhibition-dependent repair of Alzheimer's pathophysiology. Proc. Natl. Acad. Sci. 114, 8631–8636.

Larner, A., Doran, M., 2006. Clinical phenotypic heterogeneity of Alzheimer's disease associated with mutations of the presenilin–1 gene. J. Neurol. 253, 139–158.

Latulippe, J., Lotito, D., Murby, D., 2018. A mathematical model for the effects of amyloid beta on intracellular calcium. PLoS One 13, e0202503.

Lehre, K.P., Rusakov, D.A., 2002. Asymmetry of glia near central synapses favors presynaptically directed glutamate escape. Biophys. J. 83, 125–134.

Lewerenz, J., Maher, P., 2015. Chronic glutamate toxicity in neurodegenerative diseases—what is the evidence? Front. Neurosci. 9, 469.

Mackenzie, I.R., Miller, L.A., 1994. Senile plaques in temporal lobe epilepsy. Acta Neuropathol. 87, 504–510.

Mormino, E.C., Brandel, M.G., Madison, C.M., Marks, S., Baker, S.L., Jagust, W.J., 2012. Aβ deposition in aging is associated with increases in brain activation during successful memory encoding. Cereb. Cortex 22, 1813–1823.

Morris, J.C., Storandt, M., Miller, J.P., McKeel, D.W., Price, J.L., Rubin, E.H., Berg, L., 2001. Mild cognitive impairment represents early-stage Alzheimer disease. Arch. Neurol. 58, 397–405.

Morris, J.C., Roe, C.M., Grant, E.A., Head, D., Storandt, M., Goate, A.M., Fagan, A.M., Holtzman, D.M., Mintun, M.A., 2009. Pittsburgh compound B imaging and prediction of progression from cognitive normality to symptomatic Alzheimer disease. Arch. Neurol. 66, 1469–1475.

Mrdjen, D., Fox, E.J., Bukhari, S.A., Montine, K.S., Bendall, S.C., Montine, T.J., 2019. The basis of cellular and regional vulnerability in alzheimer's disease. Acta Neuropathol. 138, 729–749.

Nation, D.A., Sweeney, M.D., Montagne, A., Sagare, A.P., D'Orazio, L.M., Pachicano, M., Sepehrband, F., Nelson, A.R., Buennagel, D.P., Harrington, M.G., et al., 2019. Blood–brain barrier breakdown is an early biomarker of human cognitive dysfunction. Nat. Med. 25, 270–276.

O'Leary, T., Wyllie, D.J., 2011. Neuronal homeostasis: time for a change? J. Physiol. 589, 4811–4826.

Olsson, B., Lautner, R., Andreasson, U., Öhrfelt, A., Portelius, E., Bjerke, M., Hölttä, M., Rosén, C., Olsson, C., Strobel, G., et al., 2016. CSF and blood biomarkers for the diagnosis of Alzheimer's disease: a systematic review and meta-analysis. Lancet Neurol. 15, 673–684.

Palop, J.J., Mucke, L., 2009. Epilepsy and cognitive impairments in Alzheimer disease. Arch. Neurol. 66, 435–440.

Palop, J.J., Mucke, L., 2010. Amyloid-β–induced neuronal dysfunction in Alzheimer's disease: from synapses toward neural networks. Nat. Neurosci. 13, 812–818.

Palop, J.J., Mucke, L., 2016. Network abnormalities and interneuron dysfunction in Alzheimer disease. Nat. Rev. Neurosci. 17, 777–792.

Pascoal, T.A., Mathotaarachchi, S., Shin, M., Benedet, A.L., Mohades, S., Wang, S., Beaudry, T., Kang, M.S., Soucy, J.P., Labbe, A., et al., 2017. Synergistic interaction between amyloid and tau predicts the progression to dementia. Alzheimers Dement. 13, 644–653.

Petr, G.T., Sun, Y., Frederick, N.M., Zhou, Y., Dhamne, S.C., Hameed, M.Q., Miranda, C., Bedoya, E.A., Fischer, K.D., Armsen, W., et al., 2015. Conditional deletion of the glutamate transporter GLT-1 reveals that astrocytic GLT-1 protects against fatal epilepsy while neuronal GLT-1 contributes significantly to glutamate uptake into synaptosomes. J. Neurosci. 35, 5187–5201.

Pickett, E.K., Koffie, R.M., Wegmann, S., Henstridge, C.M., Herrmann, A.G., Colom-Cadena, M., Lleo, A., Kay, K.R., Vaught, M., Soberman, R., et al., 2016. Non-fibrillar oligomeric amyloid-β within synapses. J. Alzheimers Dis. 53, 787–800.

Pisarchik, A.N., Feudel, U., 2014. Control of multistability. Phys. Rep. 540, 167–218.

Querol-Vilaseca, M., Colom-Cadena, M., Pegueroles, J., Nuñez-Llaves, R., Luque-Cabecerans, J., Muñoz-Llahuna, L., Andilla, J., Belbin, O., Spires-Jones, T.L., Gelpi, E., et al., 2019. Nanoscale structure of amyloid-β plaques in Alzheimer's disease. Sci. Rep. 9, 1–10.

Quiroz, Y.T., Budson, A.E., Celone, K., Ruiz, A., Newmark, R., Castrillón, G., Lopera, F., Stern, C.E., 2010. Hippocampal hyperactivation in presymptomatic familial Alzheimer's disease. Ann. Neurol. 68, 865–875.

Rauch, A., La Camera, G., Luscher, H.R., Senn, W., Fusi, S., 2003. Neocortical pyramidal cells respond as integrate-and-fire neurons to in vivo–like input currents. J. Neurophysiol. 90, 1598–1612.

Rimmele, T.S., Li, S., Andersen, J.V., Westi, E.W., Rotenberg, A., Wang, J., Aldana, B.I., Selkoe, D.J., Aoki, C.J., Dulla, C.G., et al., 2021. Neuronal loss of the glutamate transporter GLT-1 promotes excitotoxic injury in the hippocampus. Front. Cell. Neurosci. 15, 788262.

Rothstein, J.D., Dykes-Hoberg, M., Pardo, C.A., Bristol, L.A., Jin, L., Kuncl, R.W., Kanai, Y., Hediger, M.A., Wang, Y., Schielke, J.P., Welty, D.F., 1996. Knockout of glutamate transporters reveals a major role for astroglial transport in excitotoxicity and clearance of glutamate. Neuron 16, 675–686.

Rusakov, D.A., Kullmann, D.M., 1998. Extrasynaptic glutamate diffusion in the hippocampus: ultrastructural constraints, uptake, and receptor activation. J. Neurosci. 18, 3158–3170.

Schneggenburger, R., Neher, E., 2005. Presynaptic calcium and control of vesicle fusion. Curr. Opin. Neurobiol. 15, 266–274.

Scimemi, A., Meabon, J.S., Woltjer, R.L., Sullivan, J.M., Diamond, J.S., Cook, D.G., 2013. Amyloid β 1–42 slows clearance of synaptically released glutamate by mislocalizing astrocytic GLT-1. J. Neurosci. 33, 5312–5318.

Selkoe, D.J., Hardy, J., 2016. The amyloid hypothesis of alzheimer's disease at 25 years. EMBO Mol. Med. 8, 595–608.

Shapson-Coe, A., Januszewski, M., Berger, D.R., Pope, A., Wu, Y., Blakely, T., Schalek, R. L., Li, P., Wang, S., Maitin-Shepard, J., et al., 2021. A connectomic study of a petascale fragment of human cerebral cortex. bioRxiv 446289.

Skaper, S.D., Evans, N.A., Soden, P.E., Rosin, C., Facci, L., Richardson, J.C., 2009. Oligodendrocytes are a novel source of amyloid peptide generation. Neurochem. Res. 34, 2243–2250.

Slepchenko, B.M., Terasaki, M., 2004. Bio-switches: what makes them robust? Curr. Opin. Genet. Dev. 14, 428–434.

Sperling, R.A., Aisen, P.S., Beckett, L.A., Bennett, D.A., Craft, S., Fagan, A.M., Iwatsubo, T., Jack Jr., C.R., Kaye, J., Montine, T.J., et al., 2011. Toward defining the preclinical stages of Alzheimer's disease: recommendations from the National Institute on Aging-Alzheimer's Association workgroups on diagnostic guidelines for Alzheimer's disease. Alzheimers Dement. 7, 280–292.

Stargardt, A., Swaab, D.F., Bossers, K., 2015. The storm before the quiet: neuronal hyperactivity and aβ in the presymptomatic stages of Alzheimer's disease. Neurobiol. Aging 36, 1–11.

Sweeney, M.D., Sagare, A.P., Zlokovic, B.V., 2018. Blood–brain barrier breakdown in Alzheimer disease and other neurodegenerative disorders. Nat. Rev. Neurol. 14, 133–150.

Syková, E., Nicholson, C., 2008. Diffusion in brain extracellular space. Physiol. Rev. 88, 1277–1340.

Syková, E., Voříšek, I., Antonova, T., Mazel, T., Meyer-Luehmann, M., Jucker, M., Hájek, M., Or, M., Bureš, J., 2005. Changes in extracellular space size and geometry in APP23 transgenic mice: a model of Alzheimer's disease. Proc. Natl. Acad. Sci. 102, 479–484.

Targa Dias Anastacio, H., Matosin, N., Ooi, L., 2022. Neuronal hyperexcitability in Alzheimer's disease: what are the drivers behind this aberrant phenotype? Transl. Psychiatry 12, 257.

Ten Kate, M., Dicks, E., Visser, P.J., van der Flier, W.M., Teunissen, C.E., Barkhof, F., Scheltens, P., Tijms, B.M., Initiative, A.D.N., 2018. Atrophy subtypes in prodromal Alzheimer's disease are associated with cognitive decline. Brain 141, 3443–3456.

Todd, A.C., Hardingham, G.E., 2020. The regulation of astrocytic glutamate transporters in health and neurodegenerative diseases. Int. J. Mol. Sci. 21, 9607.

Tong, H., Zhang, X., Meng, X., Xu, P., Zou, X., Qu, S., 2017. Amyloid-beta peptide decreases expression and function of glutamate transporters in nervous system cells. Int. J. Biochem. Cell Biol. 85, 75–84.

Tzingounis, A.V., Wadiche, J.I., 2007. Glutamate transporters: confining runaway excitation by shaping synaptic transmission. Nat. Rev. Neurosci. 8, 935–947.

van Oostrum, M., Blok, T.M., Giandomenico, S.L., tom Dieck, S., Tushev, G., Fürst, N., Schuman, E.M., 2023. The proteomic landscape of synaptic diversity across brain regions and cell types. Cell 186 (24), 5411–5427.

Veeraraghavalu, K., Zhang, C., Zhang, X., Tanzi, R.E., Sisodia, S.S., 2014. Age-dependent, non-cell-autonomous deposition of amyloid from synthesis of β-amyloid by cells other than excitatory neurons. J. Neurosci. 34, 3668–3673.

Viola, K.L., Klein, W.L., 2015. Amyloid β oligomers in alzheimer's disease pathogenesis, treatment, and diagnosis. Acta Neuropathol. 129, 183–206.

Vossel, K.A., Beagle, A.J., Rabinovici, G.D., Shu, H., Lee, S.E., Naasan, G., Hegde, M., Cornes, S.B., Henry, M.L., Nelson, A.B., et al., 2013. Seizures and epileptiform activity in the early stages of Alzheimer disease. JAMA Neurol. 70, 1158–1166.

Vossel, K.A., Tartaglia, M.C., Nygaard, H.B., Zeman, A.Z., Miller, B.L., 2017. Epileptic activity in Alzheimer's disease: causes and clinical relevance. Lancet Neurol. 16, 311–322.

Vossel, K., Ranasinghe, K.G., Beagle, A.J., La, A., Pook, K.A., Castro, M., Mizuiri, D., Honma, S.M., Venkateswaran, N., Koestler, M., et al., 2021. Effect of levetiracetam on cognition in patients with Alzheimer disease with and without epileptiform activity: a randomized clinical trial. JAMA Neurol. 78, 1345–1354.

Walsh, D.M., Selkoe, D.J., 2020. Amyloid β-protein and beyond: the path forward in Alzheimer's disease. Curr. Opin. Neurobiol. 61, 116–124.

Wang, B., Dudko, O.K., 2021. A theory of synaptic transmission. Elife 10, e73585.

Wang, L., Li, P., Hou, M., Zhang, X., Cao, X., Li, H., 2021. Construction of a risk prediction model for Alzheimer's disease in the elderly population. BMC Neurol. 21, 1–10.

Winchester, L.M., Harshfield, E.L., Shi, L., Badhwar, A., Khleifat, A.A., Clarke, N., Dehsarvi, A., Lengyel, I., Lourida, I., Madan, C.R., et al., 2023. Artificial intelligence for biomarker discovery in Alzheimer's disease and dementia. Alzheimers Dement. 19, 5860–5871.

Wyssenbach, A., Quintela, T., Llavero, F., Zugaza, J.L., Matute, C., Alberdi, E., 2016. Amyloid β-induced astrogliosis is mediated by β1-integrin via NADPH oxidase 2 in Alzheimer's disease. Aging Cell 15, 1140–1152.

Young, A.L., Marinescu, R.V., Oxtoby, N.P., Bocchetta, M., Yong, K., Firth, N.C., Cash, D. M., Thomas, D.L., Dick, K.M., Cardoso, J., et al., 2018. Uncovering the heterogeneity and temporal complexity of neurodegenerative diseases with subtype and stage inference. Nat. Commun. 9, 4273.

Zhang, X., Mormino, E.C., Sun, N., Sperling, R.A., Sabuncu, M.R., Yeo, B.T., Initiative, A. D.N., 2016. Bayesian model reveals latent atrophy factors with dissociable cognitive trajectories in Alzheimer's disease. Proc. Natl. Acad. Sci. 113, E6535–E6544.

Zhu, F., Cizeron, M., Qiu, Z., Benavides-Piccione, R., Kopanitsa, M.V., Skene, N.G., Koniaris, B., DeFelipe, J., Fransen, E., Komiyama, N.H., et al., 2018. Architecture of the mouse brain synaptome. Neuron 99, 781–799.

Zott, B., Konnerth, A., 2023. Impairments of glutamatergic synaptic transmission in Alzheimer's disease. Semin. Cell Dev. Biol. 139, 24–34.

Zott, B., Simon, M.M., Hong, W., Unger, F., Chen-Engerer, H.J., Frosch, M.P., Sakmann, B., Walsh, D.M., Konnerth, A., 2019. A vicious cycle of β amyloid–dependent neuronal hyperactivation. Science 365, 559–565.